Research Article

Effect of fine structure and pore volume in the Marimo-like carbon cathode material on the oxygen reduction reaction for the polymer electrolyte fuel cell

M. Shiraishi[1,2] · M. Inamoto[2,3] · K. Nakagawa[2,4] · T. Ando[2,5] · M. Nishitani-Gamo[2,6]

Received: 21 October 2022 / Accepted: 18 January 2023
Published online: 01 February 2023

Abstract
We measured the rotating ring-disk electrode (RRDE) voltammetry curves of a Pt catalyst supported on Marimo-like carbon (MC) to clarify the effect of carbon nanofilaments (CNFs) morphology and fine structures consisting of MC cathode material on the oxygen reduction reaction (ORR) activity for Polymer electrolyte fuel cells. The specific surface area and pore volume of MCs are influenced by their morphology and fine structures. MCs grown with Ni–Cu bimetal catalyst (represented as Ni80Cu20MC), having an octopus-like morphology, yielded four times larger total pore volume than that measured from the MC grown with Ni catalyst (Ni100MC). In the case of Ni80Cu20MC, coin-stacked graphenes perpendicular to the filament axis formed CNFs. Ni100MC consists of cup-stacked CNFs. The difference in the graphene stacked fine structure resulted in a different number of graphene edges covering the CNF surface; however, both supported Pt particle sizes and their distributions were similar. Linear sweep voltammetry with a RRDE revealed that the Pt/Ni80Cu20MC ORR onset potential was higher than that observed from the Pt/Ni100MC. This value is suggested to be correlates with the ORR activity. The origin of the ORR difference was discussed on the basis of the structural difference in the MCs.

Keywords Marimo-like carbon · Carbon nanofilament · Polymer electrolyte fuel cell · Cathode · Pt · RRDE · ORR · Catalyst support

1 Introduction

Polymer electrolyte fuel cells (PEFC) generate clean electric power from water formation energy with an efficiency ratio of more than 80%. The redox reaction occurs at the Pt electrode catalyst, consisting of a membrane electrode assembly (MEA) [1]. Carbon black is widely used as a Pt catalyst support material. A higher crystallinity of the support material is desirable for a long-range lifetime and a higher power generation performance [2], and prompt water removal from the system is also important [3].

We reported a durable, higher electrocatalytic activity on Marimo-like carbon (MC) supported Pt for a PEFC electrode catalyst [4]. The MC is a novel spherical carbon, consisting of carbon nanofilaments (CNFs) formed by the catalytic decomposition of hydrocarbons over transition metal catalysts supported on oxidized diamond powder [5]. CNFs are fixed on the diamond support surface, and a space volume formed by the CNFs is maintained to allow

✉ M. Nishitani-Gamo, mngamo@toyo.jp | [1]Graduate School of Science and Engineering, Course of Applied Chemistry, Toyo University, Saitama, Japan. [2]Research Institute of Industrial Technology, Toyo University, Saitama, Japan. [3]Saitama Industrial Technology Center (SAITEC), Saitama, Japan. [4]Department of Chemical Engineering, Kansai University, Osaka, Japan. [5]National Institute for Materials Science (NIMS), Ibaraki, Japan. [6]Department of Applied Chemistry, Toyo University, Saitama, Japan.

for water drainage. The filament fine structure is a cup-stacked or coin-stacked structure formed by many graphenes, namely, the crystallinity of CNF is much higher than that of carbon black. Several graphene edges exist on the CNF surface, and they play an indispensable role in highly dispersed Pt support sites. We assumed and studied whether the unique structural characteristics of MC, consisting of several graphene edges on the CNF surface and an appropriate space volume formed by the CNFs for the material transport such as fuel gas and water drain, could improve the MEA performance compared to that obtained using a commercially available Pt catalyst supported on the carbon black [6].

The morphology and fine structure of a fibrous carbon nanomaterial are strongly affected by the physicochemical states of the catalyst, such as the type of transition metal, its chemical states, and the addition of the second elements [7]. Catalytic growth of carbon filament using bimetal catalysts, such as Ni–Cu [8–10], Fe–Cu [11], and Co–Cu [12] was used and the effect of Cu addition on the carbon filament growth was discussed. Bernardo and coworkers reported that the Ni–Cu bimetal catalyst yielded "Octopus carbon," such as multiple CNF growths from a single catalyst particle [9]. We found that adding 20 wt% of Cu to the Ni catalyst resulted in an MC with several CNFs generated from a single catalyst particle, resembling an octopus, and established growth conditions to control the number of CNFs grown from a single catalyst particle [13]. This growth process can realize a well-controlled space volume formed by the CNFs consisting of MC, and we expect that it can assist to develop the PEFC performance, as the space plays an indispensable role in supporting gas diffusion and removing water produced by the redox reaction.

In this study, we measured the rotating ring-disk electrode (RRDE) voltammetry curves of Pt catalyst supported on the MCs, one is grown with Ni catalyst, and the other with Ni–Cu catalyst to determine the effect of CNF morphology and fine structures, consisting of the MC as a Pt catalyst support on the oxygen reduction reaction (ORR) activity.

2 Experimental

2.1 MC consists of a different type of CNFs for Pt support material

The details of the MC synthesis procedure were described in a previous report [13]. Our systematic study revealed that the oxidized diamond-supported Ni catalyst produced a cup-stacked structure, whereas Ni–Cu catalyst, with an 80 wt% Ni and 20 wt% Cu ratio produced four or five multiple CNF growths from a single catalyst particle, namely, an octopus-like CNF, with a platelet structure (also known as a coin-stacked structure). The reaction gas was methane, and the reaction time was 3 h. The reaction temperature was 550 °C for the Ni catalyst and 600 °C for the Ni80Cu20 catalyst. In this study, MC synthesized using oxidized diamond-supported Ni100 and Ni80–Cu20 catalysts are referred to as Ni100MC and Ni80Cu20MC, respectively.

The structure of the MC depended on the composition of the catalyst used for the synthesis. Scanning electron microscopy (SEM; Regulus 8230, Hitachi High-Tech Corporation, Tokyo, Japan) was used to examine the morphology of the obtained MC. The SEM images of the synthesized MCs are shown in Fig. 1. The brighter points represent the metal catalyst particles. In the case of Ni100MC, single carbon nanofilament growth from a single catalyst particle is shown in Fig. 1a. For Ni80Cu20MC shown in Fig. 1b, multiple carbon nanofilaments grow from a single catalyst particle-like as an octopus. The role of added Cu for the multiple CNF growths is suggested to yield an inhomogeneous composition of Ni–Cu particles, and we speculate that the particle having a partially covered surface with Cu, resulted in the multiple CNFs growths [13].

Numerous spaces were observed among the CNFs shown in Fig. 1. The space volume, a pore volume formed by the CNFs, is critical to water drainage and gas diffusion,

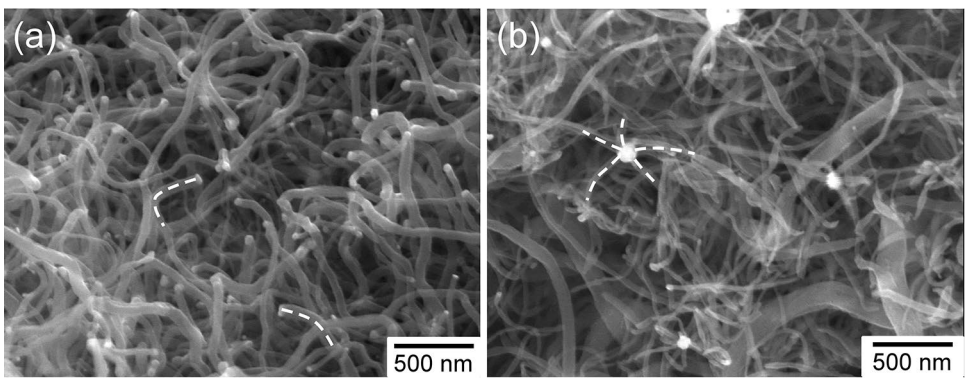

Fig. 1 Differences in the morphology of the MCs of **a** Ni100MC: One CNF was grown from one catalyst particle, **b** Ni80Cu20MC: multiple CNFs were grown from one catalyst particle

as stated in a previous section. The specific surface area and porous characterization of MCs using N_2 adsorption at 77 K were performed using Bel-sorp Mini (Microtrac BEL Corp.) [14]. The Brunauer–Emmett–Teller (BET) equations were used to determine the apparent surface area (S_{BET}), and the Barrett–Joyner–Halenda method was used to calculate the pore volume. The morphology, fine structure, surface area, and three types of pore volumes of the Ni100MC and Ni80u20MC are summarized in Table 1. The S_{BET} of Ni80Cu20MC is almost 1.8 times higher than that of Ni100MC. The total pore volume (V_{total}) of Ni80Cu20MC is four times larger than that of Ni100MC. The macropore, having 50 nm or more in size, and volume (V_{macro}) of Ni80Cu20MC is 7.6 times larger than that of Ni100MC. The mesopore, ranging from 2 to 50 nm in size, and the volume (V_{meso}) of Ni80Cu20MC is also 2.7 times larger than that of Ni100MC. These pore volumes affected the larger V_{total} of Ni80Cu20MC. These pores of Ni80Cu20MC correlate with the octopus-like morphology. This larger space volume of Ni80Cu20MC can promote the transport of product water and fuel gas because the Ni100MC is used for the Pt support material to fabricate MEA in the PEFC [15, 19].

We revealed a difference in a graphene-stacked fine structure of CNFs consisting of the MCs using transmission electron microscopy (TEM; JEM-2100, JEOL Ltd.). The nanostructures of the MCs synthesized from these different catalysts, differ from each other. The TEM images of the synthesized MCs are shown in Fig. 2. The white lines represent a part of the stacked graphene. CNFs grown from Ni100 catalysts had a cup-stacked structure (Fig. 2a); the oriented graphene sheets indicated around 35 degrees to the fiber axis, indicated as $sin\theta_{Ni100}$. However, the CNFs grown from Ni80Cu20 catalysts had a coin-stacked structure; the graphene sheets were oriented at an angle of 90 degrees with respect to the fiber axis ($sin\theta_{Ni80Cu20}$). Therefore, CNFs grown from Ni80Cu20 catalysts have more graphene edges per unit surface area than Ni100. The distance between graphene edges is $d/sin\theta$, where θ is the angle between the fiber axis and graphene and d is the face spacing of graphite. Therefore, the number of graphene edges per unit length, n is $sin\theta/d$. The ratio of the values of n for Ni100 and for Ni80Cu20 is $n_{Ni80Cu20}/n_{Ni100} = 1/sin\theta_{Ni100} = 1/sin35° = 1.7$. The estimated number of edges included in Ni80Cu20MC per unit surface area was almost 1.7 times larger than those in Ni100MC. The graphene edges are critical to Pt particle support sites and realize a highly dispersed, narrower Pt diameter distribution, as well.

2.2 Preparation of the Pt-supported MC

The modified nanocolloidal method was used to load Pt particles onto the MC. The preparation flow of the Pt-supported MC is shown in Fig. 3. The actual number of Pt loadings was determined using thermogravimetry (Exstar TG/DTA6200, Seiko Instruments Inc.). Rapid combustion of the sample causes a powder to float in the platinum pan, resulting in an artifact effect in the TG

Table 1 The characteristics of the Marimo-like carbons for the RRDE measurement

	Used catalyst Carbon yield/mol/mol Ni	Morphology	Orientation of graphite	S_{BET} (m^2/g)	V_{micro} (mL/g)	V_{meso} (mL/g)	V_{macro} (mL/g)	V_{total} (mL/g)
Ni100MC	Ni100(5wt%)/O-dia 531.1	Whisker carbon	Cup-stacked	81	0.02	0.09	0.05	0.16
Ni80Cu20MC	Ni80Cu20(5wt%)/O-dia 623.4	Octopus carbon	Platelet (Coin-stacked)	148	0.02	0.24	0.38	0.64

S_{BET}: BET surface area, V_{micro}: Micropore volume (< 2 nm), V_{meso}: Mesopore volume (2–50 nm), V_{macro}: Macropore volume (> 50 nm), V_{total}: Total pore volume

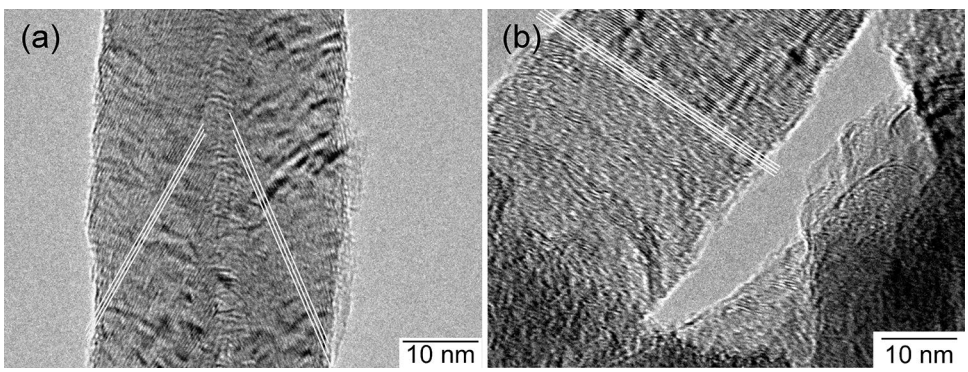

Fig. 2 TEM images of the MC nanostructure. **a** Ni100MC consists of CNFs with a cup-stacked structure. **b** Ni80Cu20MC consists of CNFs with a platelet, coin-stacked structure. This structure difference was mainly due to a Cu addition to the Ni catalyst for the MC growth [13]

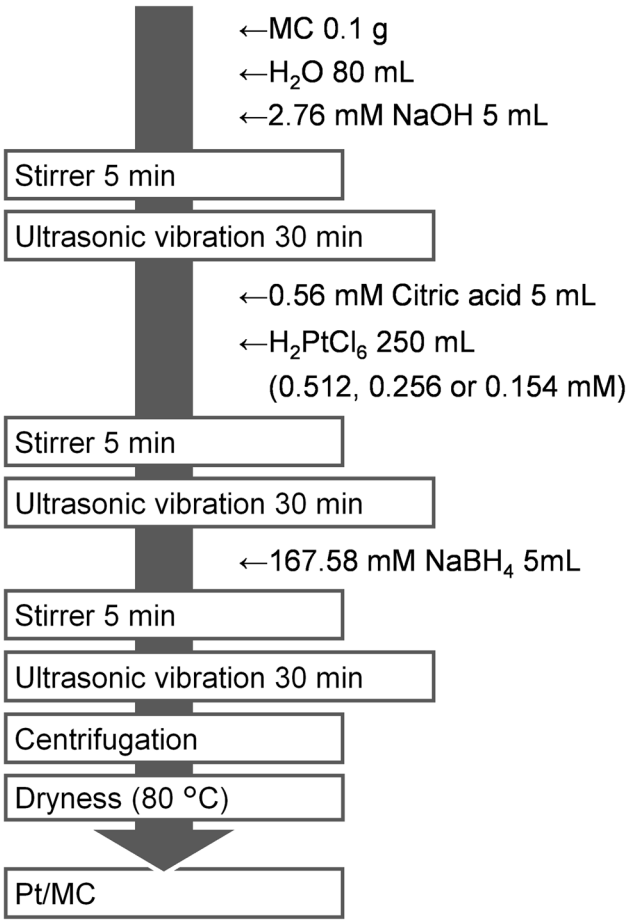

Fig. 3 Preparation flow of the MC-supported Pt catalyst

curve. To prevent such failure, the temperature increase rate was decreased in the duration of a large weight loss rate. For Ni100MC, the temperature was raised from room temperature to 480 °C at 5 °C/min, from 480 to 640 °C at 1 °C/min, and finally from 640 to 900 °C again at 5 °C/min. For the Ni80Cu20MC, the temperature was increased from room temperature to 380 °C at 5 °C/min, then from 380 to 560 °C at 1 °C/min, and finally from 560 to 900 °C again at 5 °C/min. The remaining weight after the measurement was considered the amount of Pt, and the weight ratio of Pt loadings to MCs was calculated.

2.3 Electrochemical measurements with RRDE

For the half-cell ORR measurements, the catalyst ink was prepared by ultrasonically irradiating 10 mg of the MC-supported Pt catalyst, 0.45 mL of a propanol solution, and 32 µL of 5 wt% Nafion solution for 15 min. The ratio of Nafion to catalyst was determined using a previous report [15]. We also used a commercially available catalyst (TEC10E50E; Tanaka Kikinzoku Kogyo K.K. Pt loadings 46.7 wt%), which is a Pt catalyst supported on carbon black for an MEA electrode to prepare a catalyst ink. It was prepared with 0.45 mL of propanol solution and 54-µL of 5 wt% Nafion solution using 10 mg of the TEC10E50E catalyst. A Glassy carbon disk electrode was polished, ultrasonically cleaned in water, and dried. A 5.04-µL catalyst ink was pipetted onto the disk electrode and dried at 55 °C for 1 h to form a catalyst thin film followed by drying at room temperature for 15 min. Table 2 summarizes the amount of Pt on the disk electrode used for the RRDE measurements.

For the RRDE measurements, a Hg/Hg_2SO_4 electrode (MSE) in saturated K_2SO_4 solution was used as the reference electrode, the counter electrode was platinum wire, and the electrolyte solution was O_2 saturated 0.1-M $HClO_4$. The ORR current was measured by sweeping the potential from 0.4 to − 0.59 V (vs MSE) at 10 mV/s at the rotation rates of 100, 400, 900, 1600, and 2500 rpm. All potentials in this study, however, refer to that of the reversible hydrogen electrode.

3 Results and discussions

3.1 Pt particles supported states over the MCs

Figure 4 shows TEM images of the MC-supported Pt catalyst. The effect of CNF fine structure on the supported states of the Pt particles when the amount of Pt is almost the same, and (a) Ni100MC is a cup-stacked structure, (b) Ni80Cu20MC is a coin-stacked one, is shown in Fig. 4a and b, respectively. Although the CNF fine structure between Ni100MC and Ni80Cu20MC differs, the Pt particle size and the loaded density are comparable. The average Pt diameter is estimated in the range of 2–4 nm. The loaded Pt

Table 2 The amount of Pt on the disk electrode used for the RRDE mesurements

Sample	The amount of Pt on the disk electrode (µg)	The concentration of Pt on the disk electrode (µg/cm^2)
Pt(7.2 wt%)/Ni100MC	7.53	38.41
Pt(14.8 wt%)/Ni80Cu20MC	15.32	78.17
Pt(11.9 wt%)/Ni80Cu20MC	12.57	64.12
Pt(6.9 wt%)/Ni80Cu20MC	7.43	37.92
TEC10E50E(Pt 46.7 wt%)	46.23	235.88

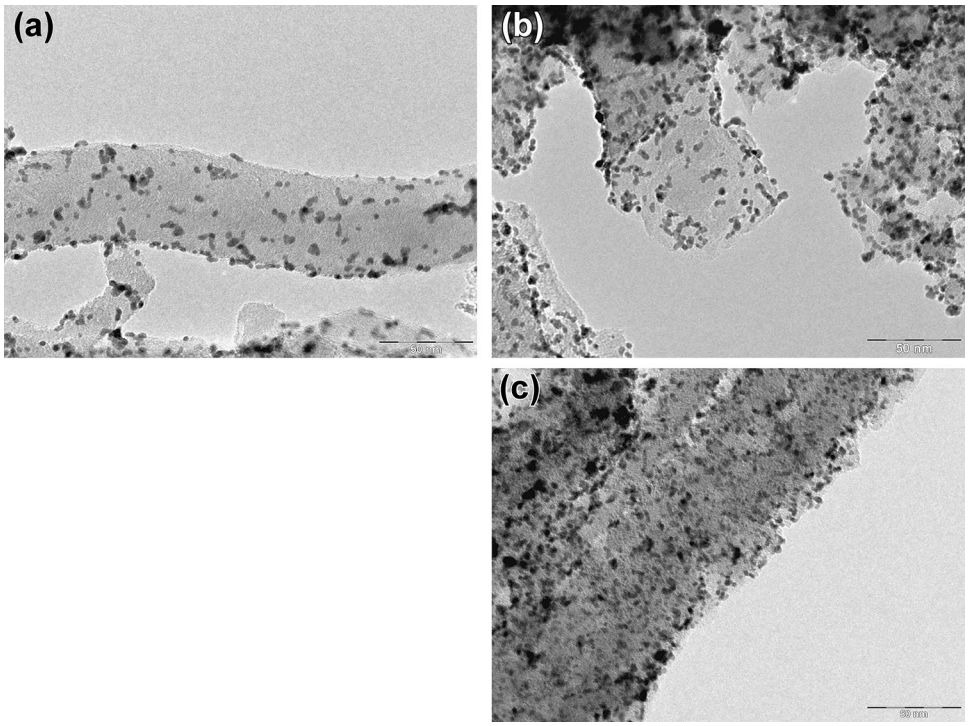

Fig. 4 TEM images of the Pt/MCs. **a** Pt(7.2 wt%)Ni100MC, **b** Pt(6.9 wt%)Ni80Cu20MC, and **c** Pt(14.8 wt%)Ni80Cu20MC

ratio increased twice higher in the case of 14.8 wt% Pt-loaded Ni80Cu20MC (Fig. 4c) than in the case of 6.9 wt% (Fig. 4b), and the Pt loaded increased density and particle average size are comparable (Fig. 4a and b). We measured the size and number of Pt particles in the TEM images and described histograms to better understand the Pt particle diameter distribution. The histograms of the loaded Pt particle diameter distribution obtained from TEM images of (a) Pt(7.2 wt%)Ni100MC, (b) Pt(6.9 wt%)Ni80Cu20MC, and (c) Pt(14.8 wt%)Ni80Cu20MC, are shown in Fig. 5. These histograms show a similar profile and a peak in the range of 2–4 nm. These Pt-supported states were similar, but the MC fine structure and the amount of supported Pt differ. Both Ni100MC and Ni80Cu20MC include several graphene edges on the CNF surface. These edges provide Pt support sites for achieving uniform, dispersive Pt support states on the CNF surface.

3.2 ORR measurements using the RRDE method

Figure 6 shows the ring electrode currents of rotating ring-disk electrode voltammetry for the ORR of the samples shown in Table 2. We also measured the TEC10E50E (Tanaka Kikinzoku Kogyo K.K. Pt loadings 46.7 wt%) at the same time as a reference. The ring electrode currents of Pt/Ni80Cu20MC was very small in the same level of TEC10E50E, and while the Pt/Ni100MC indicated two times higher currents, the value is also small, as shown in Fig. 6. The measured ring currents suggest that the side reaction can be negligible in this study. We calculate number of electrons transferred of Pt/MCs and TEC10E50E catalysts with using Koutecky-Levich equation, as shown in Table 3. The value is in the range from 3.3 to 3.8 obtained from Pt/MCs and around at 3.6 calculated from TEC10E50E. These results suggest that a four-electron reaction mainly occurred with negligible two-electron reaction.

Figure 7 shows the RRDE voltammetry curves for the ORR of Pt(7.2 wt%)Ni100MC (red line), and Pt(6.9 wt%) Ni80Cu20MC (blue line). We determined the ORR starting potential as the measured current density reached 5% of the limited current density**,** calculated as 4.0 mA/cm^2. In the case of Pt(7.2 wt%)Ni100MC, the ORR start potential was 0.87 V, and in the case of Pt(6.9 wt%)Ni80Cu20MC, it was 0.90 V. The higher ORR starting potential indicates a higher Pt activity. The Pt catalyst loaded on the Ni80Cu20MC is more active than in the case of Ni100MC on the ORR. The Pt particle size distributions of Pt(7.2 wt%) Ni100MC and Pt(6.9 wt%)Ni80Cu20MC were similar (Fig. 5). The difference in the ORR starting potential between Pt(7.2 wt%)Ni100MC and Pt(6.9 wt%)Ni80Cu20MC is not explained by the Pt particle size distribution, but rather by a fine structure difference in Ni100MC and Ni80Cu20MC, particularly, the number of graphene edges. Tsuji and coworkers reported that the PtRu catalyst particle size did not affect the oxidation reactivity of methanol when different structures of CNFs were used [16]. Bessel and coworkers also studied the effect of a support material structure on the Pt catalyst activity in methanol oxidation [17]. They

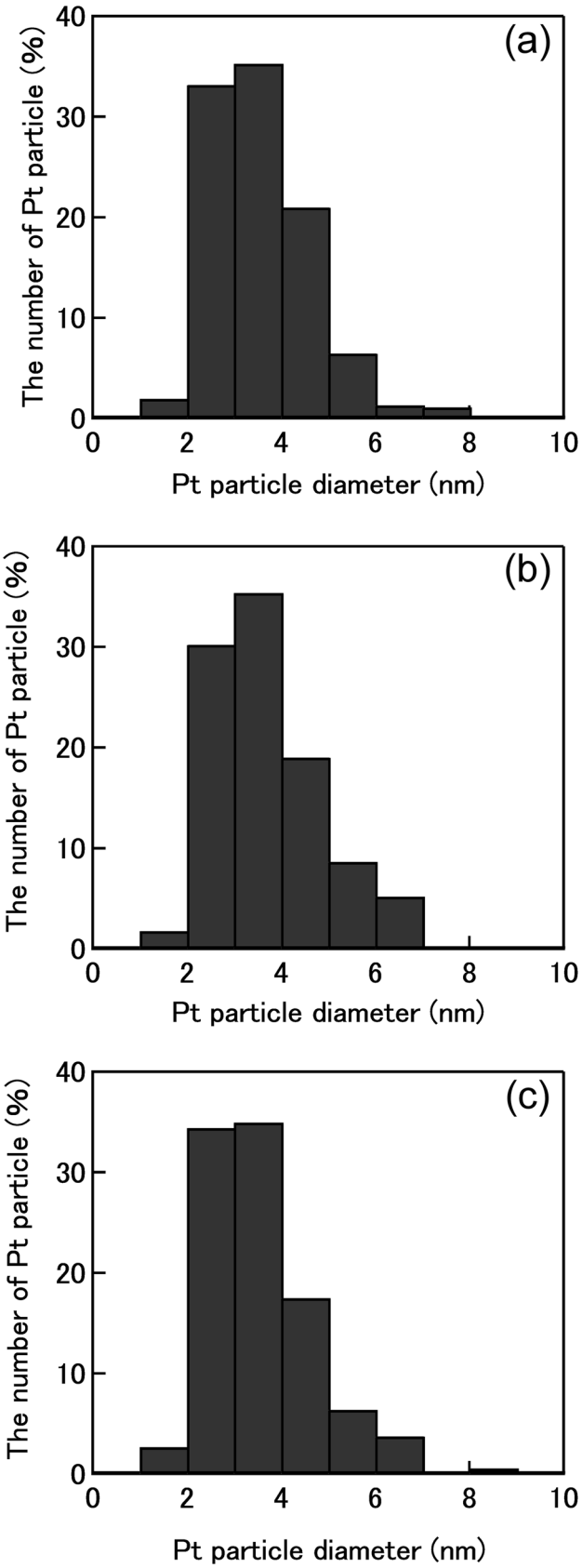

Fig. 5 A diameter distribution of the Pt particles supported on the MCs. **a** Pt(7.2 wt%)Ni100MC, **b** Pt(6.9 wt%)Ni80Cu20MC, and **c** Pt(14.8 wt%)Ni80Cu20MC

reported that a fine support material structure, such as a stacked graphene orientation of CNFs, caused a variation in Pt crystallinity, implying that the Pt catalyst activity should be varied. Zheng and coworkers revealed that the electronic state of CNF-supported Pt catalysts is affected by the difference in the CNF fine structure using X-ray photoelectron spectroscopy [18]. They speculated that the CNF fine structure influenced the interaction between Pt catalysts and the support material, with a stronger interaction, resulting in higher Pt catalytic activity for the ORR. We also observed a higher ORR onset potential which correlates to the catalytic activity using Ni80Cu20MC as a support material. The number of graphene edges of Ni80Cu20MC is estimated to be 1.7 times larger than that of Ni100MC, and there may be a stronger interaction between Pt particles and Ni80Cu20MC, and the interaction possibly affected the higher ORR activity.

The possible higher Pt activity for the ORR using Ni80Cu20MC support also correlates with the specific surface area and porous characteristics of the MC shown in Table 1. The specific surface area of Ni80Cu20MC is 1.8 times larger than that of Ni100MC; simultaneously, the total pore volume of Ni80Cu20MC is almost four times higher than that of Ni100MC. We have reported that the MEA fabricated with the Ni100MC supported Pt catalyst had a good cell performance in the PEFC compared to the case of using amorphous carbon supported Pt catalyst, especially in the high current density range; the pores consist of CNFs can assist material transfer in the electrode catalyst [19]. By analogy from the MEA performance fabricated with the Pt/Ni100MC, the pores with tens of nanometers included in Ni80Cu20MC can aid in material transfer, and the Pt catalyst loaded over Ni80Cu20MC can produce a higher ORR starting potential. We expect that such a pore structure of Ni80Cu20MC can effectively enhance not only gas diffusion but also prompt water removal from the PEFC system, as used for the Pt support material in the MEA cathode. We have been fabricating MEA using Ni80Cu20MC as a Pt support material to measure its cell performance expecting for a durable and higher electric power generation performance.

The amount of loaded Pt over Ni80Cu20MC affected the ORR starting potential. The linear sweep voltammetric results for the different amounts of Pt loaded over Ni80Cu20MC are shown in Fig. 8. The results obtained from the TEC10E50E (Tanaka Kikinzoku Kogyo K.K. Pt loadings 46.7 wt%) are also shown as a reference in Fig. 8. In the case of loaded Pt at 6.9 wt%, the ORR starting potential was 0.90 V. As the Pt amount increases, the potential

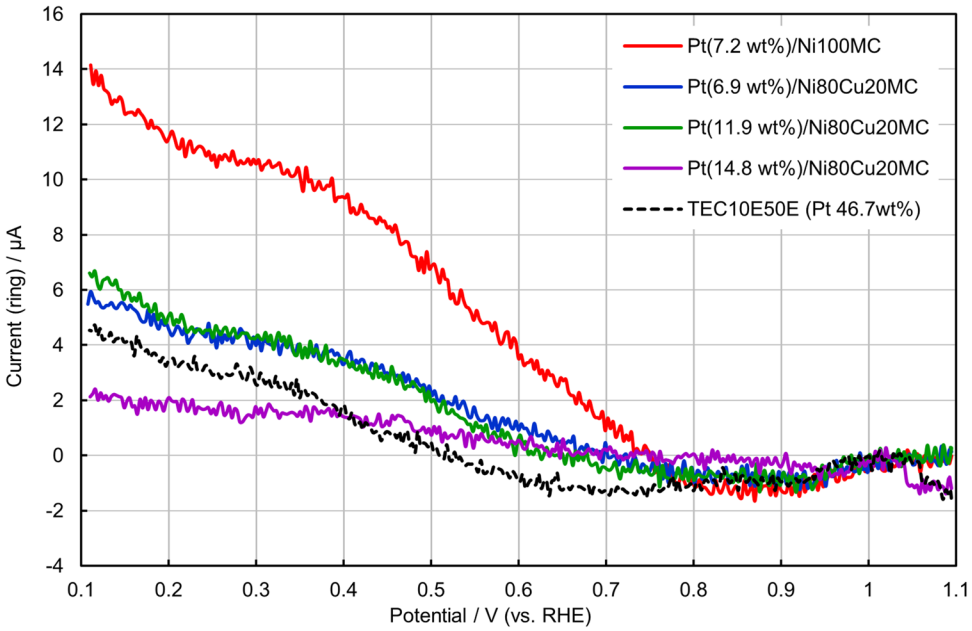

Fig. 6 The ring electrode currents of rotating ring-disk electrode voltammetry for the oxygen reduction reaction in an O_2-saturated 0.1-M $HClO_4$ solution over the samples shown in Table 2. The scan rate is 10 mV/s at 900 rpm. The results obtained from Pt-loaded MCs as Pt(7.2 wt%) Ni100MC (red line), Pt(6.9 wt%)Ni80Cu20MC (blue line), Pt(11.9 wt%)Ni80Cu20MC (green line), and Pt(14.8 wt%) Ni80Cu20MC (purple line) are indicated. The TEC10E50E (Tanaka Kikinzoku Kogyo K.K. Pt loadings 46.7 wt%) result is also shown as a reference with a black dotted line

Table 3 Number for electrons transferred of Pt/MCs and commercially avairable Pt/C catalyst

Sample	Number of electrons transferred
Pt(7.2 wt%)/Ni100MC	3.67
Pt(6.9 wt%)/Ni80Cu20MC	3.79
Pt(11.9 wt%)/Ni80Cu20MC	3.63
Pt(14.8 wt%)/Ni80Cu20MC	3.34
TEC10E50E (Pt loadings 46.7 wt%)	3.59

increased as 11.9 wt% Pt yielded 0.92 V, and 14.8 wt% Pt yielded 0.95 V. The increase in loaded Pt over Ni80Cu20MC is attributed to an increase in the ORR starting potential or the ORR activity. The TEC10E50E produced an ORR starting potential of 0.91 V; the potential of Pt(14.8 wt%)/Ni80Cu20MC was 0.95 V and it was comparable to that obtained using the TEC10E50E. Although the amount of loaded Pt over Ni80Cu20MC was almost a 1/3 less than that of Pt included in the TEC10E50E, the ORR activity of Pt(14.8 wt%)/Ni80Cu20MC is superior to that of TEC10E50E. The

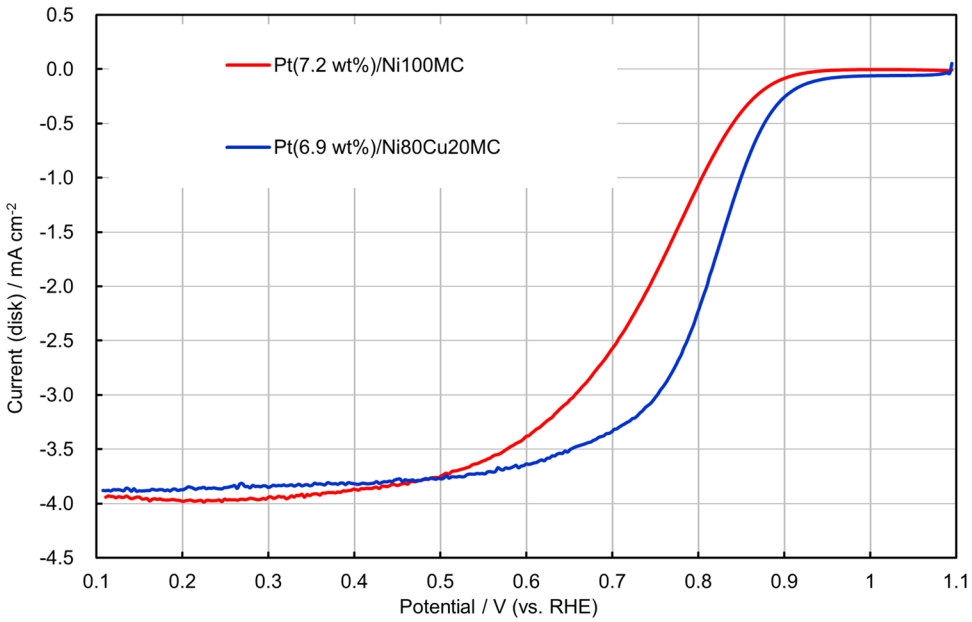

Fig. 7 Rotating ring-disk electrode voltammograms for the oxygen reduction reaction in an O_2-saturated 0.1-M $HClO_4$ solution over Pt-loaded Ni100MC (Pt(7.2 wt%) Ni100MC; red line) and Pt(6.9 wt%)Ni80Cu20MC (blue line). The scan rate is 10 mV/s at 900 rpm

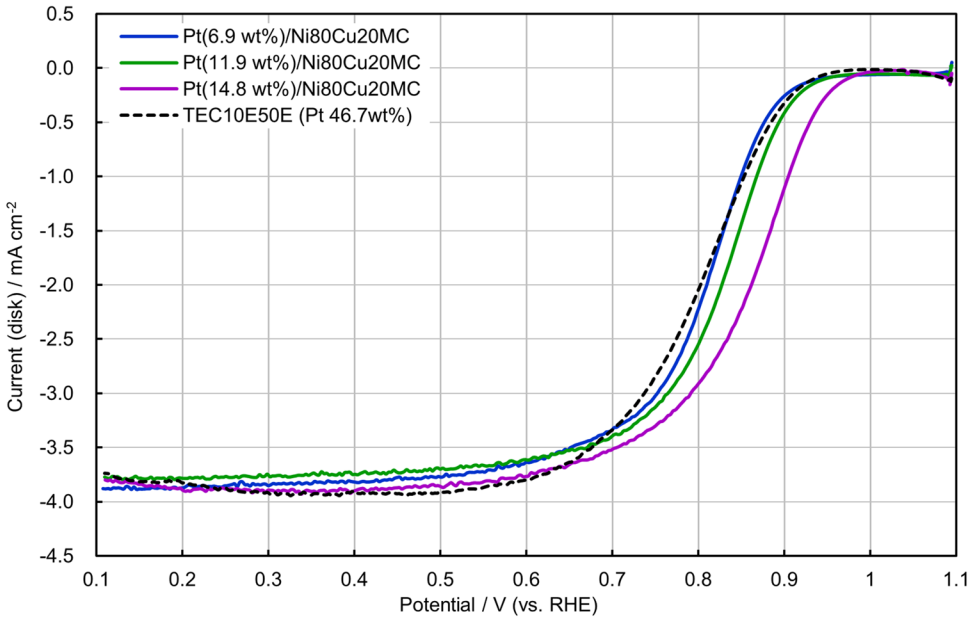

Fig. 8 Rotating ring-disk electrode voltammograms for the oxygen reduction reaction over various Pt ratios of Pt/Ni80Cu20MC in an O_2-saturated 0.1-M $HClO_4$ solution. The scan rate is 10 mV/s at 900 rpm

Pt/Ni80Cu20MC catalyst suggests realizing a PEFC with less Pt and higher electrochemical performance.

4 Summary

In this study, we performed linear sweep voltammetry using the RRDE for the Pt/Ni100MC and Pt/Ni80Cu20MC to determine the effect of CNF morphology and the fine structure consisting of the MCs as a Pt catalyst support material on the ORR onset potential values which reflect the ORR activity. FESEM analysis of the Ni80Cu20MC reveals an octopus-like morphology. TEM analysis revealed that the Ni80Cu20MC CNF fine structure was coin-stacked, whereas that of Ni100MC was a cup-stacked structure. Both fine structures provide several graphene edges on the CNF surface and a highly dispersed and narrow-diameter distribution of Pt particles supported on the MCs. A strong interaction between Pt particles and Ni80Cu20MC may exist because of more quantity of graphene edges, and the interaction can yield a higher ORR starting potential than in the case of Pt/Ni100MC. The specific surface area and porous characterization of MCs by N_2 adsorption at 77 K revealed that the pores with tens of nanometers in the Ni80Cu20MC are more than four times greater than that in Ni100MC. These pores of Ni80Cu20MC correlate with the octopus-like morphology. They can aid in material transfer, and the Pt catalyst supported on Ni80Cu20MC can produce a higher ORR starting potential which possibly represents a higher ORR activity. Such pore structures of Ni80Cu20MC can enhance not only gas diffusion but also prompt water removal from the PEFC system as used in the Pt support material in the cathode. The Pt/Ni80Cu20MC catalyst is suggested to be better candidate for MEA in PEFC. We have been fabricating MEA using the Ni80Cu20MC as a Pt support material to realize a superior PEFC with a durable and higher electric power generation performance. At the same time, to clarify the electrochemical characteristics of MCs, such as a Pt mass activity and ECSA, is necessary and important for fabricating and characterizing MEA.

Acknowledgements The study was supported by a Grant from Japan Keirin Autorace foundation (JKA) and the INOUE ENRYO Memorial Grant, TOYO University. The authors would like to thank Crimson Interactive Pvt. Ltd. for a careful review in English proofreading.

Autor Contributions MS performed linear sweep voltammetry using the RRDE for the Pt/Ni100MC and Pt/Ni80Cu20MC to determine the effect of CNF morphology and the fine structure consisting of the MCs as a Pt catalyst support material on the ORR activity. She pulled together all of the raw data to make charts and graphs for considering the effect of fine structure and pore volume on the ORR for PEFC cathode material. MI proceeded these electrochemical measurements with MS using his system, and made suggestions to determine an appropriate experimental conditions. KN designed the reactor and made suggestions to improve controllability of the growth parameter settings and to characterize the S_{BET} and pore volumes of MCs. TA is a deputy supervisor of MS doctoral dissertation and he gave important suggestions for promoting the research with his expertise of hydrocarbon physical chemistry. MN-G is a supervisor of MS doctoral dissertation. She is also a supervisor of this research project for realizing a structure-controlled MC growth process not only to achieve higher performance of PEFC but also to explore various applications.

Funding The study was supported by a grant from Japan Keirin Autorace foundation and the INOUE ENRYO Memorial Grant, TOYO University.

Data availability The datasets generated during and/or analyzed during the current study are available from the corresponding author on reasonable request.

Declarations

Conflict of interest On behalf of all authors, the corresponding author states that there is no conflict of interest.

References

1. Cameron DS (1978) Fuel cell energy generators. Platinum catalyst used in alternative energy source. Platin Met Rev 22:38–46
2. Kharwar PS, Akula S, Sahu AK, Ramanujam K (2020) Highly durable Pt-based catalyst supported on carbon deriverd from Tamarind seeds for oxygen reduction reaction in PEM fuel cell. J Electrochem Soc 167:104515
3. Wang YJ, Fang B, Li H, Bi XT, Wang H (2016) Progress in modified carbon support materials for Pt and Pt-alloy cathode catalysts in polymer electrolyte membrane fuel cells. Prog Mater Sci 82:445–498
4. Baba K, Nishitani-Gamo M, Ando T, Eguchi M (2016) Durable Marimo-like carbon support for platinum nanoparticle catalyst in polymer electrolyte fuel cell. Electrochim Acta 213:447–451
5. Nakagawa K, Oda H, Yamashita A, Okamoto M, Sato Y, Gamo H, Nishitani-Gamo M, Ogawa K, Ando T (2009) A novel spherical carbon. J Mater Sci 44:221–226
6. Eguchi M, Okubo A, Yamamoto S, Kikuchi M, Uno K, Kobayashi Y, Nishitani-Gamo M, Ando T (2010) Preparation of catalyst for a polymer electrolyte fuel cell using a novel spherical carbon support. J Power Sources 195:5862–5867
7. Rodriguez NM (1993) A review of catalytically grown carbon nanofibers. J Mater Res 8:3233–3250
8. Nishiyama Y, Tamai Y (1974) Carbon formation on copper-nickel alloys from benzene. J Catal 33:98–107
9. Bernardo CA, Alstrup I, Rostrup-Nielsen JR (1985) Carbon deposition and methane steam reforming on silica-supported Ni–Cu catalysts. J Catal 96:517–534
10. Kim MS, Rodriguez NM, Baker RTK (1991) The interaction of hydrocarbons with copper-nickel and nickel in the formation of carbon filaments. J Catal 131:60–73
11. Krishnankutty N, Rodriguez NM, Baker RTK (1996) Effect of copper on the decomposition of ethylene over an iron catalyst. J Catal 158:217–227
12. Chambers A, Rodriguez NM, Baker RTK (1995) Modification of the catalytic behavior of cobalt by the addition of copper. J Phys Chem 99:10581–10589
13. Shiraishi M, Nakagawa K, Ando T, Nishitani-Gamo M (2022) The effect of copper on the multiple carbon nanofilaments growths by the methane decomposition over the oxidized diamond-supported nickel–copper bimetallic catalyst. SN Appl Sci 4:126
14. Akiyama S, Nakagawa K (2021) Effect of mesopores in the Marimo nanocarbon anode material on the power generation performance of direct glucose fuel cell. Carbon Trends 4:100058
15. Baba K, Iwasawa K, Eguchi M, Kobayashi Y, Kobori M, Nishitani-Gamo M, Ando T (2013) Interfacial nanostructure of the polymer electrolyte fuel cell catalyst layer constructed with different ionomer contents. Jpn J Appl Phys 52:06GD06
16. Tsuji M, Kubokawa M, Yano R, Miyamae N, Tsuji T, Jun M-S, Hong S, Lim S, Yoon SH, Mochida I (2007) Fast preparation of PtRu catalysts supported on carbon nanofibers by the microwave-polyol method and their application to fuel cells. Langmuir 23:387–390
17. Bessel CA, Laubernds K, Rodriguez NM, Baker RTK (2001) Graphite nanofibers as an electrode for fuel cell applications. J Phys Chem B 105:1115–1118
18. Zheng JS, Wang XZ, Fu R, Yang DJ, Li P, Lv H, Ma JX (2012) Microstructure effect of carbon nanofibers on Pt/CNFs electrocatalyst for oxygen reduction. Int J Hydrogen Energy 37:4639–4647
19. Eguchi M, Baba K, Iwasawa K, Nishitani-Gamo M, Ando T (2013) The Marimo carbon as a polymer electrolyte fuel cell catalyst support. Trans Mat Soc Jpn 38(3):349–352